DOI: 10.71762/v2b1-6z84

Research Paper

Construction and Assessment of Brass (CuZn30)/Low carbon Steel/Brass /Brass (CuZn30) thin Film Metal Composite in Wear Resistance, Microstructural and Mechanical Properties, Incorporating Consideration of the Impact of Annealing Temperature

Seyed Mostafa Mirtabaei[1*], Farid Bagherpoor[2]
[1]Faculty of Mechanical Engineering, Shahrood University of Technology, Shahrood, Iran
[2]School of Mechanical Engineering, College of Engineering, University of Tehran, Tehran, Iran
*Email of Corresponding Author: mirtabaee_58@yahoo.com
Received: November 19, 2024; Accepted: January 24, 2025

Abstract
Manufacturing thin metal multi-layer composites and enhancing their mechanical properties are challenging tasks. In this study, a thin-layer metal composite (500 μm) consisting of brass/ST14/brass was fabricated using the cold rolling bonding (CRB) method. To optimize its mechanical characteristics, the composite was subsequently annealed at temperatures of 450°C, 600°C, and 750°C. The resulting samples were evaluated in terms of tensile strength, microhardness, formability, wear resistance, and surface morphology using SEM/BSE imaging. The results indicated that the sample annealed at 750°C exhibited the highest formability but the lowest tensile strength and wear resistance (i.e., greatest weight loss). In contrast, the unannealed sample showed the highest tensile strength and wear resistance, but the lowest formability. Among all treatments, annealing at 600°C provided the best overall balance of mechanical performance, demonstrating superior formability, tensile strength, and wear resistance. Therefore, it can be concluded that annealing at 600°C represents the optimal treatment for the brass/ST14/brass composite in this study.

Keywords
Brass (CuZn30) /Low Carbon Steel/Brass (CuZn30) Composite, Thin Metal Composite, Annealing Temperature, Cold Rolling, Mechanical Properties

1. Introduction

The use of thicker metals with higher volume and weight is typically suggested to improve the mechanical properties of metal constructions; nevertheless, this increases the amount of metal consumed and the price, heaviness, workability, and forming difficulty. The foundation of this study is the proposal for thin metal multi-layer composites in modern science to enhance mechanical properties, which addresses the problems mentioned above and can produce suitable properties with less weight and quantity [1- 2]. Metal-based composites are a viable option for producing high-quality, multipurpose products. The enhanced mechanical features of multi-layer metal composites, such as their increased strength and reduced weight, are crucial for the industrial use of metals [3-4].

Metal composites can be made using various techniques, although most are costly and highly complex [5-6]. Hence, scientists and artisans prefer to use less expensive techniques and equipment [7]. The rolling forming method is one of the approaches that have been proposed in this field. In this sense, multi-layered metal composites can be produced using hot and cold rolling processes [8-9]. It is the primary subject of this study. The forming properties are among the most essential factors when using metals in various industries [10]. The production of multi-layer metal composites by strengthening this feature has been noticed in industrial and research fields [11]. Therefore, in this regard, the annealing process can also improve the formability by creating the recrystallization phenomenon [12-13]. As a result, this research focused on two metals frequently used in the industry, brass and low-carbon steel ST14, both of which have appropriate formability and elastic deformation behavior. St14 steel alloy has a high iron and low carbon content. This kind of steel has suitable welding, machining, and bending properties due to its low carbon content. Its use has increased exponentially as a result of these three fundamental features. St14 steel has a density of 7.85 g/cm3, and because of its high iron content, it possesses magnetic characteristics. St14 steel is frequently utilized for structural profiles. Prices for low-carbon steel are often less than those for other steel alloys and high-carbon alloy varieties. ST14 steel has an elasticity modulus of 200 GPa [14].

On the other hand, the brass alloy is an alloy of copper and zinc, divided into yellow brass, red brass, lead brass, silicon brass, tin brass, and nickel brasses based on the changes in appearance and color[15]. The solubility limit of zinc in copper is 32.5% at the freezing temperature and about 35% at the ambient temperature; therefore, the α solid solution phase is the most important microscopic network in the brass alloy. The freezing point of brass alloys can frequently be comparatively low, and the melting point of copper is lowered when additional metals are present. Put another way, the more fluid the alloy is, the lower the solidification range, although a larger volume of concentrated shrinkage typically accompanies this. Brass metal is also quite malleable, creating items requiring small-scale shaping [16-17]. This reason is one of the primary rationales behind selecting this metal for this study. Therefore, according to the above, in addition to the selection of the three-layer brass/low-carbon steel/brass composite in this study, strengthening this composite has also been suggested. In this context, the strengthening of this alloy can increase its efficiency and expand the fields of its use in industries. Therefore, rolling operations and annealing treatments have been applied in this research to increase strength and formability. Thus, this study initially manufactured a three-layer composite of brass, low-carbon steel, and brass by cold rolling the materials. The annealing processes were then carried out. The basis for the rolling process is the plastic deformation of the metals by the stress they experience when they pass through the appropriate cylinder.

The justification of the connection between the layers in the rolling forming process is based on four theories: the thin layer theory, the energy barrier theory, the diffusion bonding theory, and the recrystallization connection theory. The energy barrier theory is proposed [18]. Two theories of thin film and energy barrier theory are proposed during the cold rolling process; two theories of diffusion bonding and recrystallization connection theory are also proposed during the hot rolling and annealing treatment, depending on the applied temperature [19-20]. The theory of recrystallization connection in connection with the annealing process is proposed, considering that the annealing temperature in this research is lower than the melting point of the metals utilized [3-17-21]. On the other hand, the connections between metal layers in the rolling process are affected by several parameters: initial

sheet thickness, thickness reduction percentage, annealing time and temperature, strain percentage, rolling speed and direction, surface preparation, and crystal structure. In this research, the reduction of thickness and the change in dimensions of the sample were calculated first. Also, the shift in annealing temperature is considered a variable parameter, and the rest were considered constant.

2.1 materials

In this study, low-carbon steel St14 and 90 brass were utilized. XRF first analyzed the chemical compositions of primary metals to perform a thorough examination. The relevant findings are displayed in Table 1. Table 2 also shows the fundamental physical properties of brass and low-carbon steel.

Table 1. Chemical composition of low-carbon steel and brass (XRF results)

Zn	Cu	Fe	P	S	Mn	C	
10	90	-	-	-	-	-	brass Ms90
		99.4>	0.03	0.03	0.4	0.08	(low carbon steel- St14)

2.2 Sample preparation and manufacturing by the cold rolling method

The samples of three primary metal layers had 4.5×150×50 mm dimensions before the rolling process, as shown in Figure 1a. These samples are subjected to the cold rolling process, which is the cold rolling process, and the samples can be seen in Figures 1c and 1d, respectively. After the cold rolling process, the dimensions of the samples change; in this case, the thickness change is more than 50%, and the new dimensions of the sample are 1.5×270×70 mm.

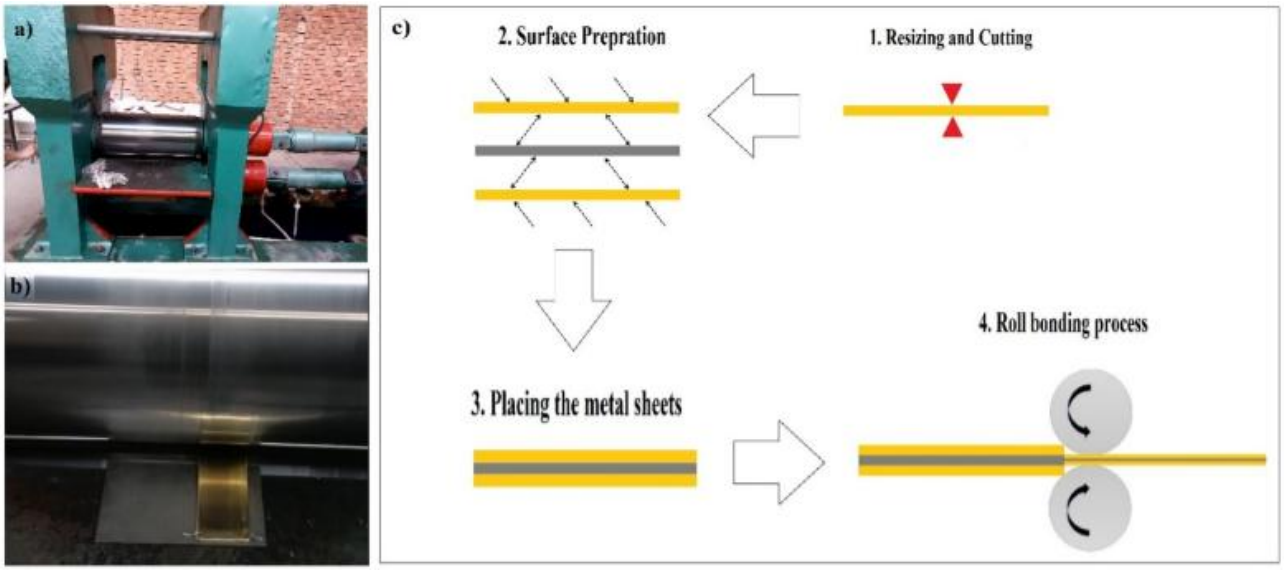

Figure 1. Cold rolling, a) rolling machine, b) rolled sample, c) schematic of the rolling process

2.3 Changing the dimensions in the rolling process

Reducing the thickness of the layers in the rolling process is one of the critical parameters in the successful investigation of composite production in the rolling process. Also, this parameter determines the number of passes in the rolling operation. In such a way, the thickness reduction by

up to about 50% or more than 50% shows the success of the rolling operation. Therefore, in this research, the thickness reduction and the change in the structure after a rolling pass have been calculated.

Y_1: Thickness before rolling operation
Y_2: Thickness after rolling operation

$$\Delta Y = Y_2 - Y_1 = 2.4 - 0.5 = 1.9$$
$$Thickness\ reduction(\%) = 1 - \frac{0.5}{2.4} = 79\ \%$$

We also have sample length to calculate the change in size:

L_1: Length before the rolling operation
L_2: Length after rolling operation

$$\Delta L = L_2 - L_1 = 34 - 15 = 19$$
$$Thickness\ reduction(\%) = 1 - \frac{0.5}{2.4} = 79\ \%$$

Calculation of the change in sample width:

Z_1: width before the rolling operation
Z_2: width after rolling operation

$$\Delta z = z_2 - z_1 = 9.25 - 5 = 4.25$$
$$Increase\ in\ width\ (\%) = 1 - \frac{9.25}{5} = 85\ \%$$

Therefore, the calculation of strains in three directions is as follows:

ε_x: Strain in the longitudinal direction
ε_y: Strain in the Thickness
ε_z: Strain in the width

$$\varepsilon_x = \frac{\Delta L}{L_1} = \frac{L_2 - L_1}{L_1} = \frac{19}{15} = +126\%$$
$$\varepsilon_y = \frac{\Delta y}{y_1} = \frac{y_2 - y_1}{y_1} = \frac{1.9}{0.5} = -380\%$$
$$\varepsilon_z = \frac{\Delta z}{z_1} = \frac{z_2 - z_1}{z_1} = \frac{4.25}{5} = +85\%$$

Therefore, based on the calculations above, the thickness reduction in the first pass equals 79%, indicating that the rolling process successfully reduced the sample's thickness. Additionally, the first pass's amount of strains is 126% along the sample's length, width, and thickness, 85% and 380%, respectively. As the computations demonstrated, the strains have grown in the length and width directions but have dramatically decreased in the thickness direction. These facts indicate that the initial attempt at altering the proportions was successful. As a result, just one pass was considered for rolling procedures in this study.

2.4 Analyzing manufactured composites

The three-layer brass/low carbon steel/brass composite used in this study was manufactured by rolling, and it was then annealed at temperatures of 450°C, 600°C, and 750°C degrees Celsius to

enhance its characteristics. In this regard, samples not annealed and annealed at 450 °C, 600 °C, and 750°C underwent analyses of forming limit, microhardness, and tensile strength. The forming and strength of the composite were examined in light of the analyses mentioned above.

- *Microhardness*

The standard Vickers microhardness test was used to determine the hardness of samples produced via cold rolling and annealing techniques. The samples' surfaces are first smoothed and polished to conduct this test. The mounted samples are then placed under the micro-hardness device along their thickness, and the stress is applied, causing a diamond-shaped effect on the piece. The rhombus diameters are measured to determine the Vickers hardness. The hardness test was performed at six distinct locations in the sample to decrease the error percentage. The results were averaged and then expressed.

- *Tensile test*

Assessing the material's behavior against tensile axial stress is one of the critical aspects of mechanical properties. The uniaxial tensile test is essential for evaluating mechanical behavior in this regard. Consequently, the uniaxial tensile test used in this study is derived from the SANTAM machine and the ASTM E8M-9 standard. The test was conducted at room temperature, with a strain rate of 1 x 10-4 s, and without lubricants. Figure 2 displays the sample's geometric shape and samples at different annealing temperatures.

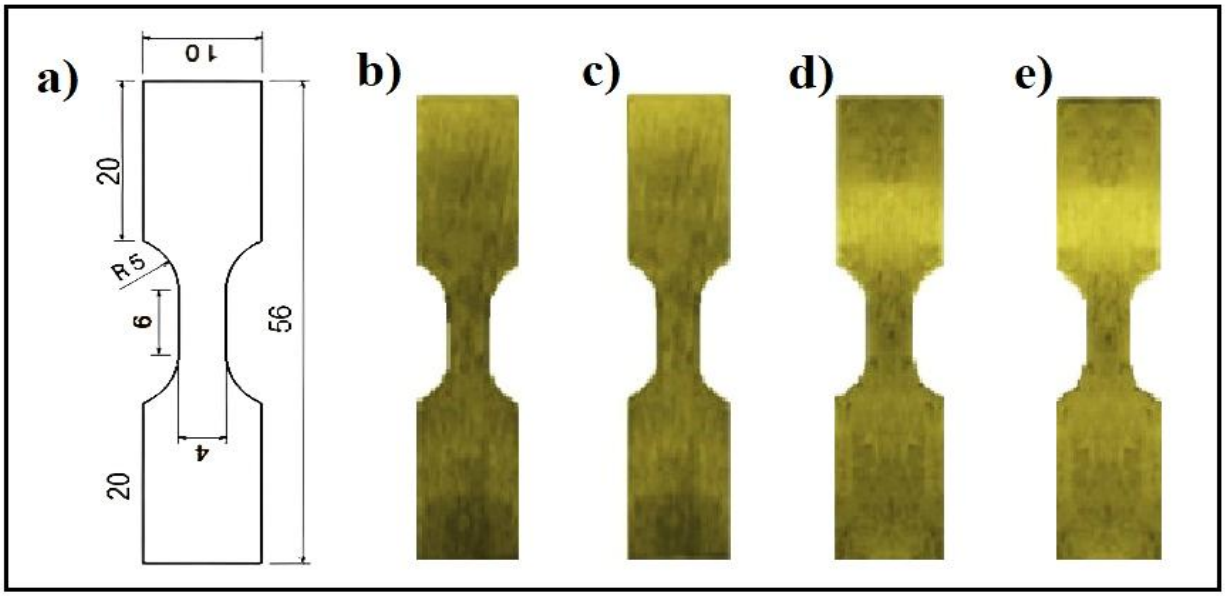

Figure 2. Tensile test samples, a) The geometric shape of the sample in the uniaxial tensile test, b) as-received, c) 450 °C, d) 600 °C, e) 750 °C

- *The forming limit diagram*

The Nakazima test was used to obtain the forming limit diagram. The Nakazima test consists of a two-piece matrix or mold for placing a three-layer sheet on it and a mandrel with a hemispherical head, which applies pressure to the sample and causes the sheet to move to the breaking point. Due to the high sensitivity of the experimental test to determine the forming limit curve, all stages of the

test—preparation of samples, measurement, calculation of large and small strains, and drawing of the forming limit diagram—must be done carefully to get the desired result.

2.4.4 Preparation of samples for the Nakazima test

The forming limit diagram (FLD) was determined utilizing eight samples. The forming limit diagram can be obtained by varying the sample width while performing the Nakazima test. Thus, the dimensions of the FLD test samples are determined based on the assumption that the mold's dimensions are quartered compared to the standard test. Samples following the intended pattern are prepared to identify the left curve, while rectangular samples are ready to determine the correct curve. The dimensions of standard samples are displayed in Figure 3. Circle gridding is the most popular kind, and it is used to carry out the gridding operation for this test.

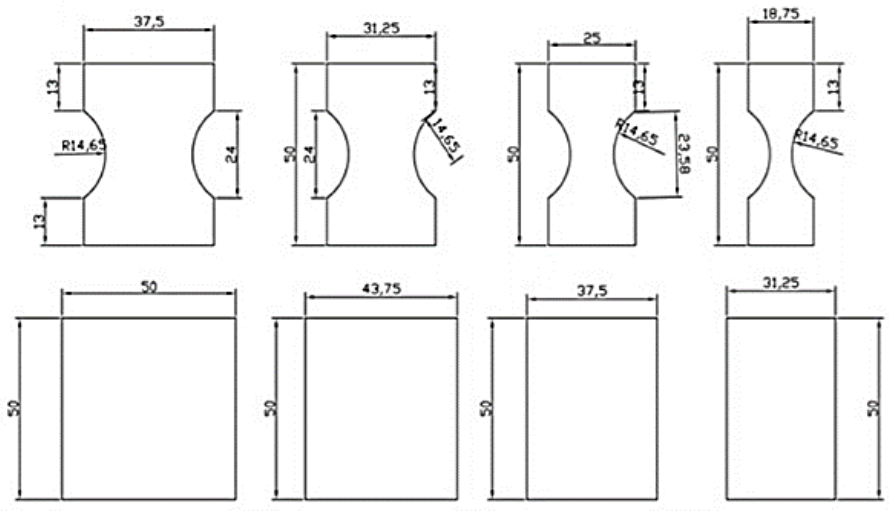

Figure 3. Pattern dimensions of the Nakazima test samples to determine FLD

- Nakazima test

The prepared samples with the mold are placed under the stretching machine; the mandrel touches the sheet's surface, and the machine's moving jaw moves the mandrel towards the sheet at a speed of 2 mm/min and causes the sheet to be stretched. The test will be stopped when the device's display shows a loss of power due to sheet breakage or tearing. This test used a 60-ton GALDABINI model tensile machine for the Nakazima test.

- Calculation of FLD

The forming limit diagram is used to measure and evaluate the formability of metal sheets. To perform the stretching process, a square or circular mesh should be printed or engraved on the surface of the sample sheet, which is equal to the deformation of two diameters of this mesh. In the throat region, obtaining small and large limit strains is possible. In this way, during the forming operation, the circular grids are deformed and become oval to calculate the principal strains ε_1 and ε_2 in the defective area, the maximum principal strain is in the direction of the large diameter of the ellipse, and the minimum principal strain is in the direction of the small diameter of the ellipse. It is considered, and its value is calculated. In this research, a microscope was used to obtain the strain. Large and small diameters were measured, and their value was calculated through the following relationships. Then,

large and small strain values were calculated for all the test samples, and the corresponding forming limit diagram was reported.

Real strains are calculated using the following equations:

d_1 large oval drop size

d_2 small oval drop size

d_0 is the initial value of the diameter.

$$\varepsilon_1 = ln(^{d_1}/_{d_0}) \quad (1)$$

$$\varepsilon_2 = \ln(^{d_2}/_{d_0}) \quad (2)$$

Engineering strains can be calculated from the following relationships:

$$e_1 = \frac{d_1 - d_0}{d_0} \quad (3)$$

$$e_2 = \frac{d_2 - d_0}{d_0} \quad (4)$$

2.5 Microhardness

Hardness is defined as the resistance of a material to plastic deformation or the sinking of a more rigid material, which is expressed by micro-hardness. Due to work hardening, the high density of dislocations creates an increase in microhardness, which is achieved by the saturation of the microhardness of the steel layers after the cumulative rolling process from the soft behavior of the material. Accordingly, sophisticated methods exist for describing the dislocation density using artificial crystal models based on the plastic strain gradient theory. It has been introduced as a crystallization dislocation model. Equation 5 shows the relationship between the dislocation density of metals and the micro-size hardness, which is used in this study.

$$\rho = \frac{HV^2}{27a^2G^2b^2} - \frac{3\sqrt{2}\sqrt{HV}\,cot\,\varphi}{\sqrt{1.72}\pi^2 b\sqrt{F}} \quad (5)$$

In this regard:

HV Vickers microhardness,

φ Vickers penetration half angle,

α experimental coefficient between 0.2 and 0.5, which is about 0.3 to work in the cumulative rolling process,

G shear elastic modulus,

b Burgers vector,

F is the applied force of the indenter

2.6 Wear resistance

This study examined wear resistance according to the ASTM G99 by pin-on-disk wear test at room temperature with a wear diameter of 13 mm, linear speed of 0.1 m/s, and 150 RPM in various sliding distances of 0, 250, 500, 750, and 1000 m.

3. Results and Discussion

3.1 Tensile strength

Figure 4a shows tensile test results. Both primary metals, steel and brass, have significantly less elastic strain than the composite samples. Also, both metals have a limited stress and low deformation range compared to other composites. Therefore, for St14 and brass, the maximum strain before failure is less than 0.5%. On the other hand, as seen in Figure 4b, the tensile strength, strain, and formability increase significantly when the CRB and annealing procedure are carried out. Higher tensile strength is observed in the rolled composite sample before annealing (as-received sample) than in other treatments. In such a way, the maximum value that the composite can withstand is equal to the stress value of the proportionality limit in the sample. Plastic deformation has been shown only before failure in a small area. Hence, the maximum strain in this composite is only 8%, corresponding to the fracture limit strain. From a 3% strain value to an 8% strain value, this composite has shown the behavior of plastic flexibility, which is a minimal range. While the tensile strength value of this composite is high, which indicates the high strength of this composite, the maximum tensile strength value is 570 MPa. Now, we check the tensile strength of composites annealed at 650 °C. Also, Figure 4b shows the stress-strain diagram of the sample annealed at a temperature of 750°C. As can be seen, the tensile strength of the composite has decreased significantly, while the formability of the composite has increased considerably. The annealed composite sample has a large plastic deformation zone, which indicates a significant increase in formability in this composite. The maximum tensile strength in this composite is 340 MPa.

Additionally, compared to the sample without annealing treatment (as-received sample), the tensile strength of all three types of annealed composites is significantly reduced, but their formability is higher. The treatment corresponding to 450°C demonstrates the lowest flexibility and the highest tensile strength among the annealed treatments due to the annealing process at low temperature. Out of all the annealed treatments, the composite with the highest formability and the lowest tensile strength is treated at 750°C. Still, when all three of these treatments are considered together, the phenomenon of recrystallization and increasing diffusion may be the reason for the comparatively slower shift in the tensile strength lowering trend between the 600°C and 750°C treatments compared to the 450°C and 600°C treatments. Also, the findings of this study are supported by the results of Tayyebi et al. [22], which are consistent with the findings of this study.

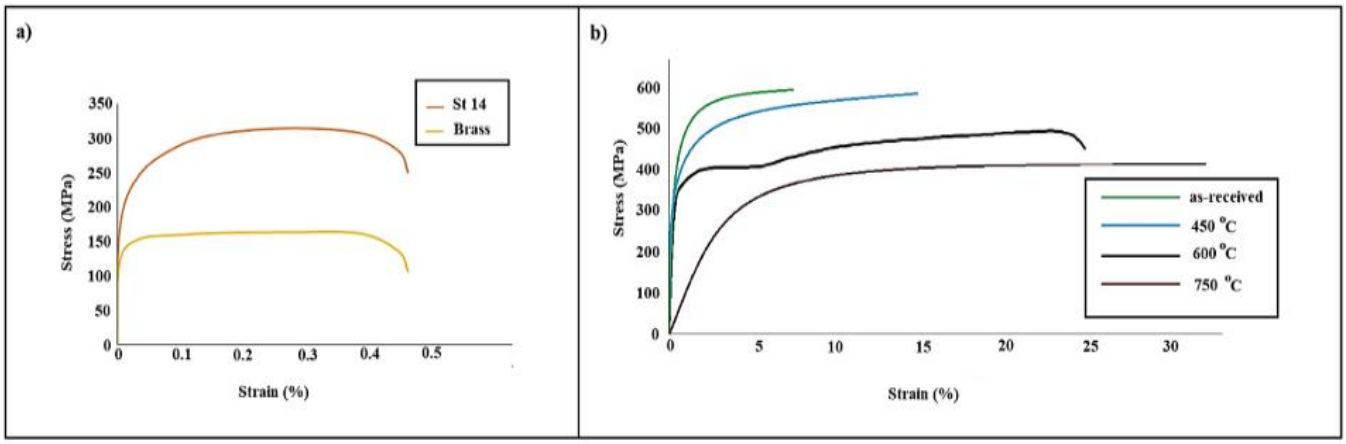

Figure 4. Stress-strain diagram, a) raw materials; b) three-layer composite samples before the annealing process (as-received), annealing at 450 °C, annealing at 600 °C, and annealing at 750 °C

3.2 Forming limit diagrams

Formability is one of the critical features in the construction of multi-layer metal composites. This feature was investigated using the Nakazima test, and the results were reported as an FLD diagram. The shape of the FLD results is based on the circle's diameter increasing and decreasing in various areas. Circles that are not burst should be used to draw the forming limit diagram. The FLD of rolled samples at ambient temperature and before the annealing treatment can be seen in Figure 5. According to Fig. 5, the surface of the curve is small, which indicates the weak forming property of the composite in this manner. This state is due to the rolled composite's high strength, flow stress, and hardness. An annealing process can improve this property. As the tensile strength has shown (Figure 4), the sample before annealing treatment has high tensile strength and a brittle fracture. FLD test results also confirm this issue. This condition can be generalized for several reasons: as a result of applying the rolling treatment, the hardness and density of the composite have increased. The bond between the layers is weak; as a result, it does not show the forming property, and the failure created will have a layered tear state. Also, as shown in Fig. 5, the amount of formability is improved by annealing at 450 °C.

The reason can be stated as follows: in this instance, the barriers preventing the dislocations from moving have been eliminated. The reason can be stated as follows: in this instance, the barriers preventing the dislocations from moving have been eliminated. The sample showed better formability at 600°C than at 450°C or without any annealing treatment due to the formation of stronger chemical bonds and recrystallization phenomena; furthermore, this ability improves at 750°C. The annealed treatment at 600°C can be observed to differ the most from the annealed treatment at 450°C. The slower trend in the temperature differential between 600 and 750°C can also be extended until the nucleation's entire expansion and the germination process's conclusion. Moreover, as shown in Figure 5, the sample that did not receive an annealing treatment has the lowest forming limit diagram among the treatments applied, indicating that this treatment is less effective than the other treatments. Furthermore, the annealing treatment boosts the forming ability, resulting in a higher forming diagram in the sample treated at 450°C than before the annealing procedure. This condition also gets better when the treatment is administered at 600°C. The forming ability increases with the annealing treatment's temperature up to 750°C, showing the best and highest forming capacity among the other

treatments. The research findings are consistent with those of Delshad et al., who support the findings above [23].

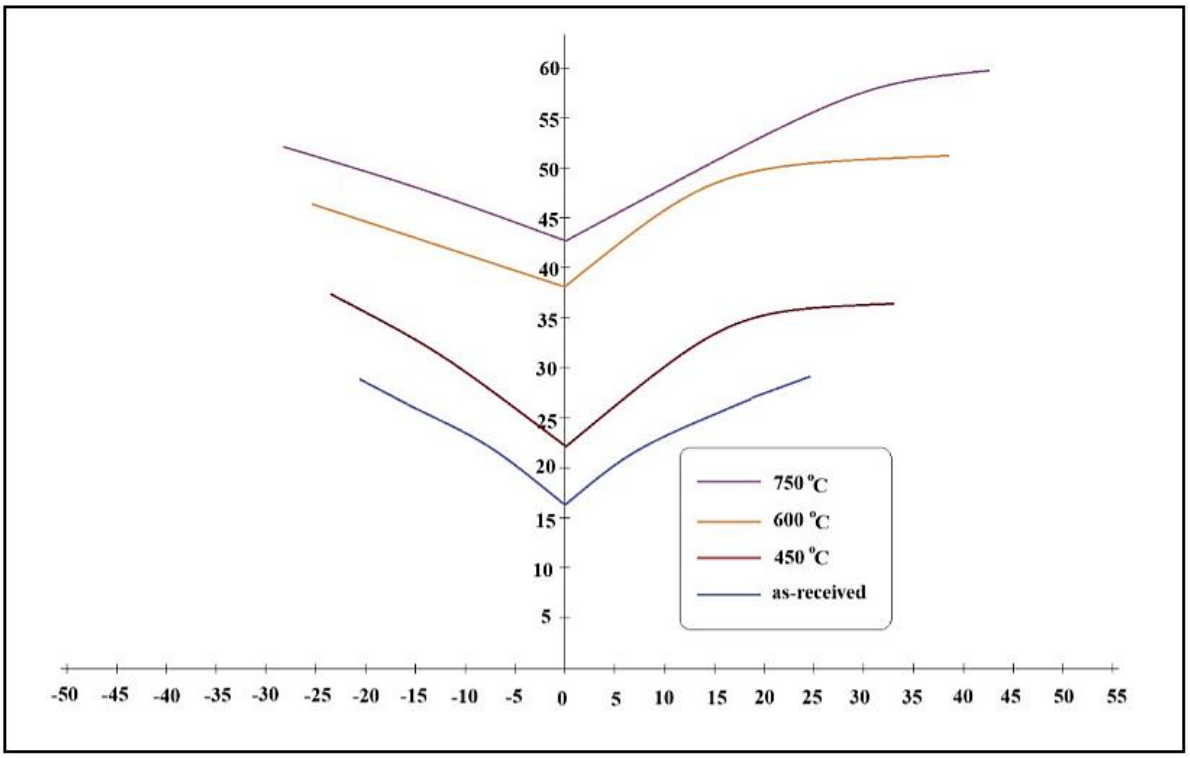

Figure 5. Nakajima test results (FLD diagram) for the sample rolled at ambient temperature and before annealing, the sample annealed at 450°C, the sample annealed at 600°C, and the sample annealed at 750°C

3.3 Microhardness

Hardness is defined as the resistance of a material to plastic deformation or the sinking of a more rigid material, which is expressed by micro-hardness [24]. Due to work hardening, the high density of dislocations increases microhardness, achieved by the saturation of the steel layers' microhardness after the material's rolling process [25]. The results are shown in Figure 7 for two layers of low-carbon steel and brass separately. As can be seen, both brass and low-carbon steel layers showed the highest Vickers hardness after cold rolling. So, they had values of 182.03 and 219.11, respectively. Additionally, the microhardness of both metals trends downward as the annealing temperature rises. Low-carbon metals have a more severe tendency in this reduction process, nevertheless. Thus, the microhardness values of low-carbon steel are reported to be 198.25, 95.42, and 89.32 HV, respectively, at temperatures of 450°C, 600°C, and 750 °C. The lowest value for the annealed sample at 750°C is 89.23 Vickers. On the other hand, brass also had a decreasing trend, so the corresponding values were measured at 450 °C, 600 °C, and 750 °C, respectively, 119.05, 100.52, and 90.41 HV. Therefore, in this regard, brass metal has also shown the lowest microhardness value of 90.14 HV in annealing at 750°C. This issue can be generalized to the entanglement of grains and recrystallization. In this case, the new grains can recrystallize freely without any distortion; in this case, microstructural evolution is formed. Figure 7 shows that after an annealing process at 600°C, the microhardness decreases with a gentle downward slope, indicating the critical point where recrystallization is complete. For both brass metal and low-carbon steel, this crucial point is at 600°C. The results

obtained in this study align with the results of Diehl et al. and Zhao et al., which confirms the results of this research [26-27].

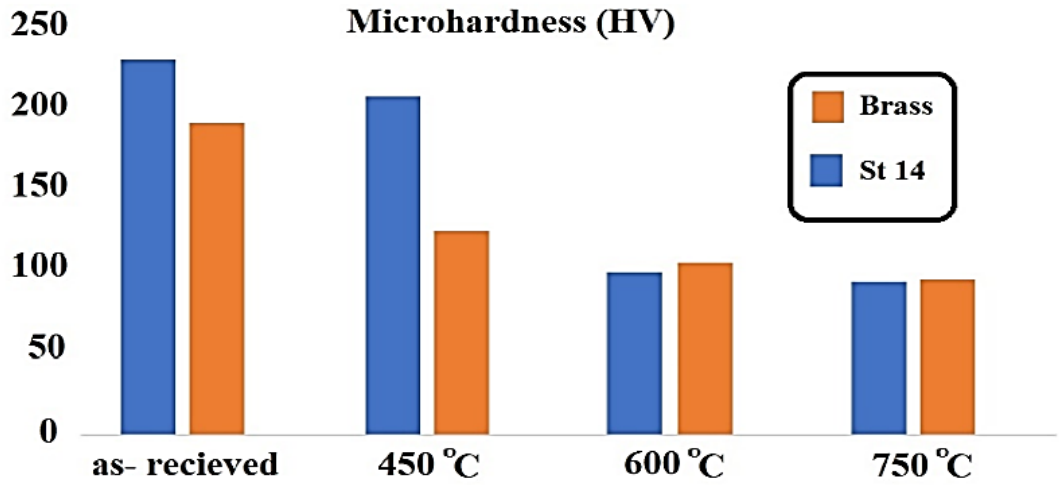

Figure 6. Microhardness of brass and low-carbon steel at different annealing temperatures

3.4 X-ray diffraction (XRD)

One of the things that directly affects and improves the plasticity properties of composites is the phenomenon of recrystallization [28]. In this phenomenon, the crystal structure of the metal composite changes. One of the factors causing such a situation in this instance is the repetition of the granulation, which can change the composite's crystal structure [29]. The annealing operation's temperature value can directly impact the crystal structure. As a result, it is essential to look at how the crystal structure changes during the annealing process temperature change, which was carried out in this study. Figure 7 shows the outcomes of the crystal structure alteration. These results are based on the respective JCDPS cards (JCPDS No. 003–1018) Cu5Zn8 alloy (JCPDS No. 025–1228), as seen in Figure 7. The as-received sample has long index peaks, indicating the structure's crystallinity. The sample without annealing treatment has a larger crystal structure than other samples, based on the XRD diagrams of other annealed samples. As can be seen, by performing the annealing process and increasing the annealing temperature, the crystal structure is degraded, and the strength and intensity of the observed peaks show a significant decreasing trend; in this regard, the sample with an annealing temperature at 750°C shows the lowest peak intensity in the crystallinity structure. Also, according to these results, comparing the 600°C annealing process with the 750°C annealing process, the crystallinity structure reduction trend is lower than in other samples. This structural change with a slight decrease in the changes after the temperature of 600°C indicates that at 600°C, the emerging critical temperature is recrystallized, which confirms the microhardness results obtained in this research. Also, the results obtained from changes in the crystallinity structure in this research align with the results of Nie et al. and Ma et al., which confirms the results of this research [30-31].

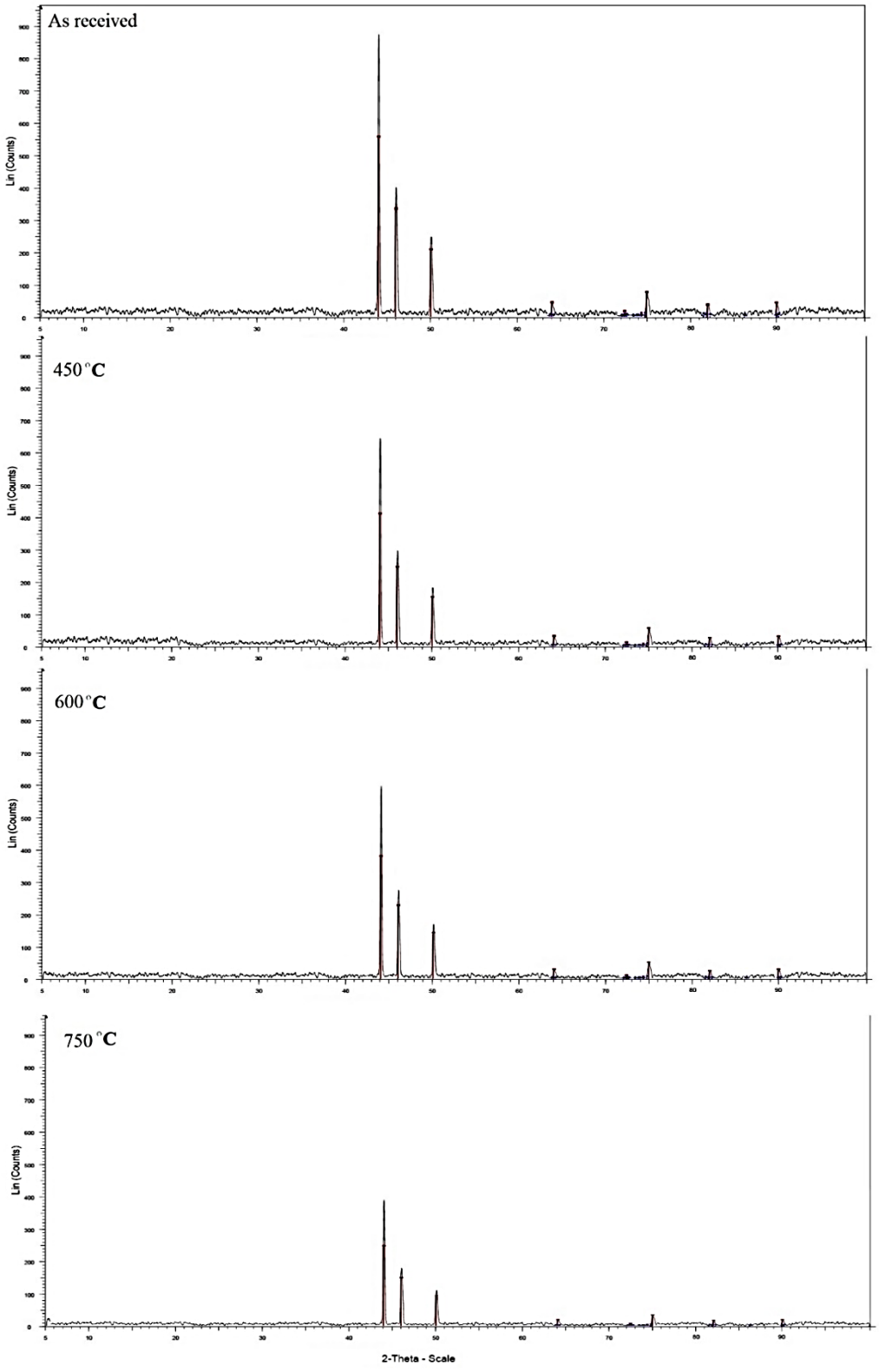

Figure 7. XRD results at various annealing temperatures: (a) as received; (b) at 450°C; (c) at 600°C; (d) at 750°C

3.5 Microstructural characterization

- SEM images

Developing an appropriate microscopic structure to join the layers is the first step toward successfully producing a composite [32]. Consequently, scanning electron microscopy (SEM) was utilized in this study to investigate the microscopic structure of the treated samples, and Figure 8 displays the findings on the samples' fracture section. As seen in Figures 8a and 8b, cracks are created in the section when the failure occurs. It indicates that the composite has poor formability and is brittle when fractured. In this case, it is possible to deduce that there was a physical rather than a chemical interaction between the layers. The surfaces connect due to the horizontal force applied, and the thin layer theory justifies the connection. The energy barrier theory is one of the other theories in line with bonding in metal layers in cold rolling. According to this theory, to connect the metal composite's layered structure, the connection barrier's energy barrier needs to be overcome to join the metal layers properly. This theory states that the cause of this high energy barrier is two metals approaching each other, which causes repulsion between these two metals, which must overcome this energy to connect. Therefore, in this regard, the necessary energy can be provided by performing the annealing process to overcome this barrier and create a stronger connection. In addition to the two theories already discussed, two more theories—the recrystallization connection theory and the diffusion bonding theory—are put forth for the heat treatment (annealing process). Therefore, we will have a change in the morphological structure compared to the as-received sample, which can be seen in Figure 8.

As can be seen, at low annealing temperatures, fewer pores are created, and as the annealing temperature increases, the amount and size of the pores created in the structure increase. Therefore, it indicates that the phenomenon of recrystallization has occurred in the composite structure. As the heat increases, the pores will become larger and deeper. As a result, among the annealed treatments at temperatures of 450, 600, and 750°C, respectively, a growing trend in pore size can be observed in Figures 8B-D. In such a way that the minimum pore size is observed in the microscope image at the annealing temperature of 450°C (Fig. 8c), the largest size of the pores in the SEM images corresponds to 750°C, which indicates the ductile failure state and high formability of the composite. Also, as the tensile strength test results are shown in Figure 4, as a result of the annealing operation, the annealed composites enter the plastic deformation phase faster than the control sample, which shows that the annealed composites are more formable than the received composites. Therefore, the results of tensile strength and SEM images confirm each other. Furthermore, the outcomes in this field agree with the results of Najafzadeh et al, so the study findings are confirmed [33].

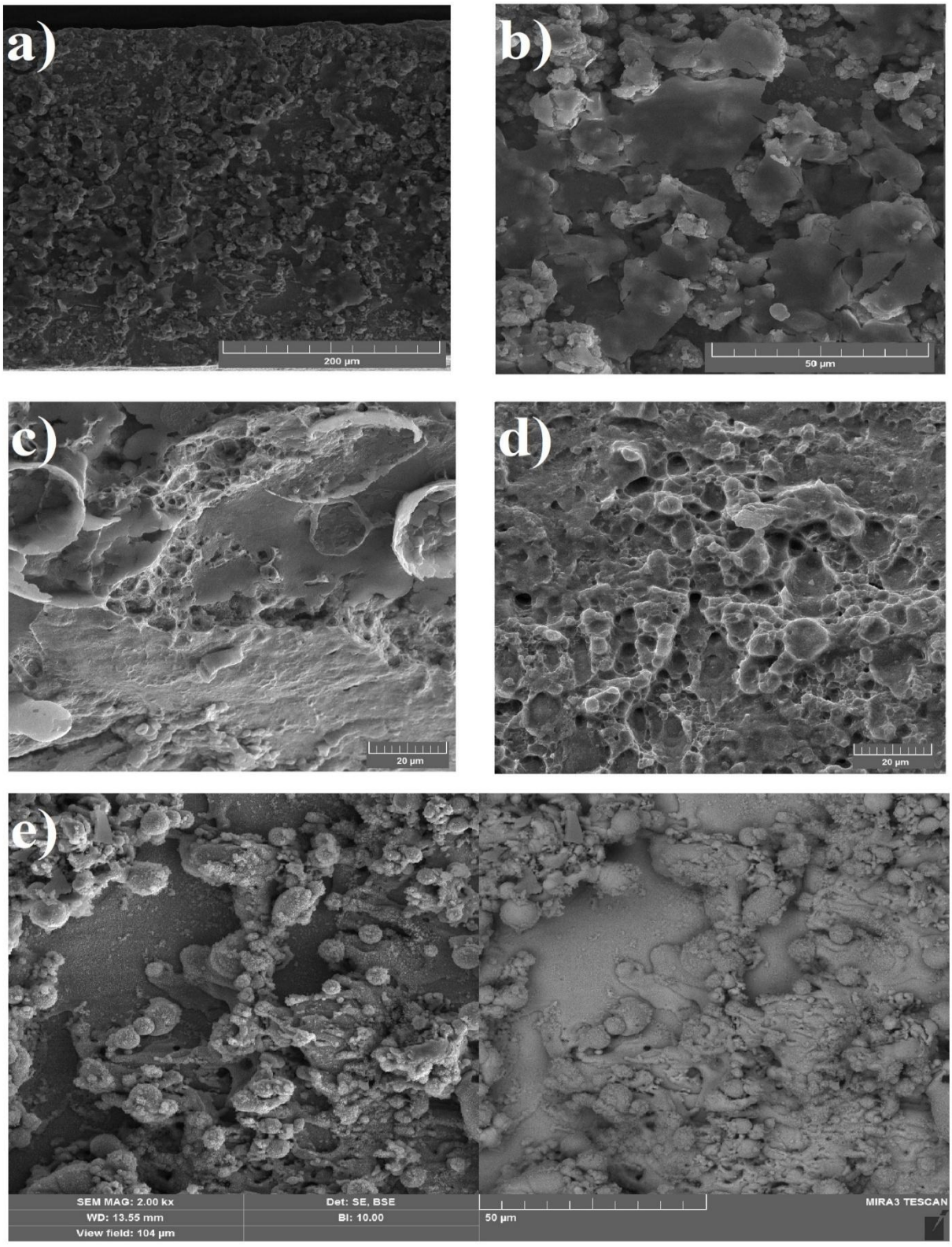

Figure 8. SEM images of three-layer composite brass 70/low carbon steel/brass 70 at different annealing temperatures, a,b) as-received; c) 450°C; d) 600°C; e) 750°C

3.6 Wear resistance

Wear resistance is an important parameter determining the life span and type of products used. As a result, this study examined the samples' wear resistance at various annealing temperatures and before annealing. In this context, SEM images of abrasion wear and the weight loss in the sliding distance values of 0, 250, 500, 750, and 1000 m have also been analyzed.

- *Loss of weight and microstructure change in wear resistance*

The weight changes, weight loss, and SEM images of the samples at various wear resistance distances are displayed in Figure 9. The dimensions of the samples were 2.5 x 2.5 cm, and the weights of the 450°C, 600°C, 700°C, and as-received samples were 1.8261, 1.8071, 1.7902, and 1.8650 grams, respectively. As shown in Figure 9, with increasing annealing temperature, the weight of the samples shows a significant decrease in the wear resistance test. This issue can be attributed to the increase in plasticity of the three-layer brass/St14/brass composite as a result of annealing heat treatment; the rise in plasticity can also be seen in the tensile test results in Figure 4, confirming this issue. Also, on the other hand, at each temperature of the annealing process (0°C, 450°C, 600°C, and 750°C), the amount of weight loss can be seen significantly due to the increase in the sliding distance. In this regard, the lowest amount of weight loss among the annealing temperatures is related to the sample from the as-received sample, which is equal to 0.0283 gr, and the highest amount of weight loss is associated with the treatment of 750°C, with the amount of weight loss being 0.0579 gr. Figure 9b shows the weight loss of the samples in different annealing temperature treatments at various sliding distances. As observed, the weight loss trend dramatically decreases with increasing sliding distance at all temperatures. However, of all the treatments, the weight loss in the 750 treatment exhibits a considerable falling slope compared to the other treatments.

Figures 9C–9F show the analysis results of the SEM (BSE) images of the as-received and annealed composites at temperatures of 450°C, 600°C, and 750°C during the wear test at the sliding distance of 1000 meters, which allowed for a more precise examination of the samples. The lowest amount of wear can be seen in Figure 9C, which is related to the sample from the as-received sample. Further, as the annealing temperature increases, more wear is visible in the images, so the sample at 750°C has the highest amount of wear among the annealing treatments. The sample with an annealing temperature of 450°C shows the lowest amount of wear compared to the annealed treatments, confirming the weight loss result in the wear resistance test (Figures 9a and 9b).

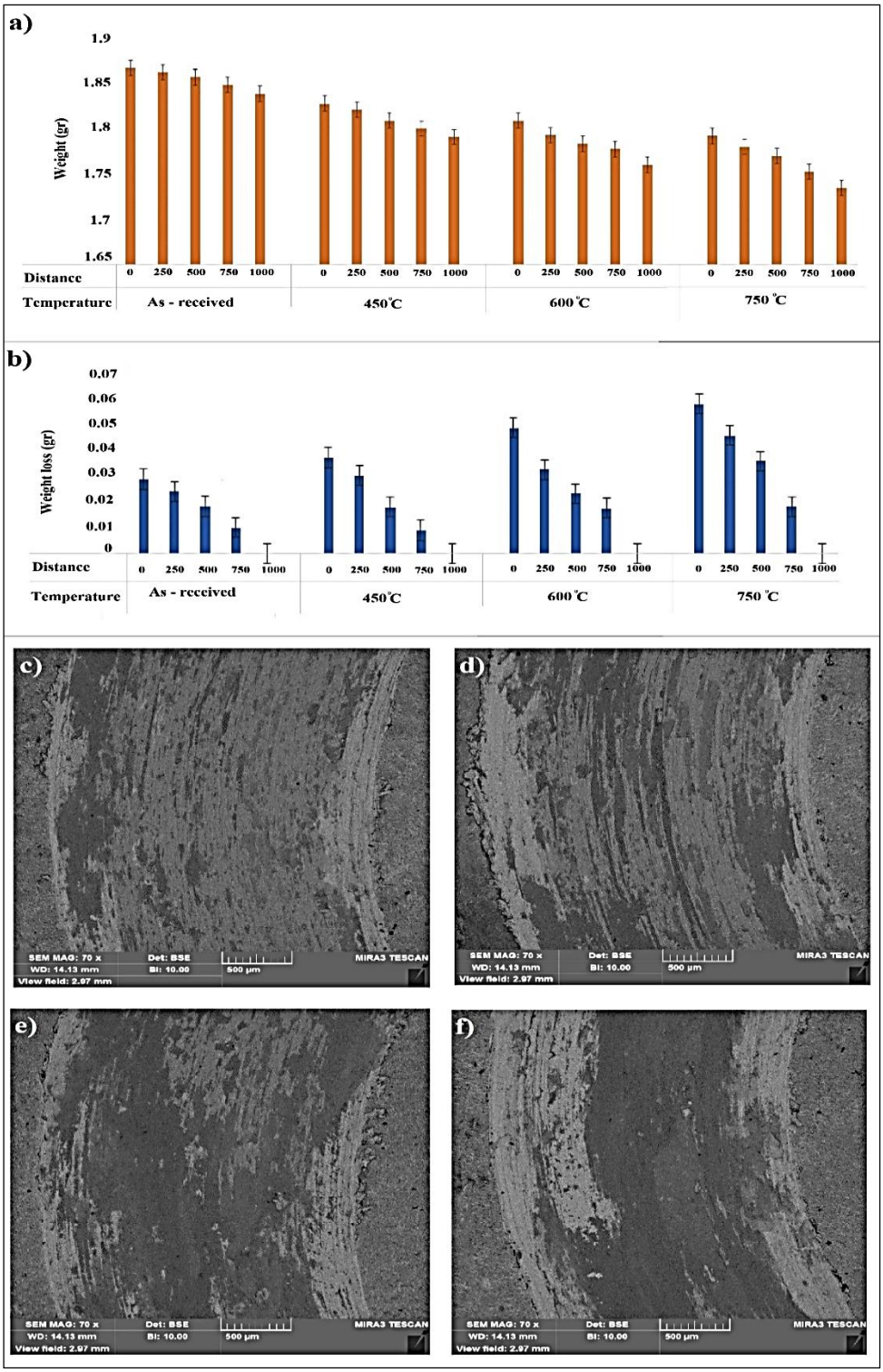

Figure 9. Wear resistance at annealing different temperatures; a) Weight of samples, b) Loss of weight, c) SEM/BSE image of the as-received sample, d) SEM/BSE image of at 450°C annealing sample, d) SEM/BSE image of at 600°C annealing sample, d) SEM/BSE image of at 750°C annealing sample

4. Conclusion

This study investigated the effect of the annealing process on formability, crystallinity, and mechanical properties of a three-layer brass/low carbon steel/brass thin film composite. The study's findings demonstrated that, in comparison to the annealed samples, the tensile strength is at its maximum level because of the cold rolling process and the occurrence of the cumulative process. The composite produced by cold rolling without annealing has the lowest formability despite having the highest ultimate strength and the least strain. Consequently, the annealing treatment is recommended in this study to enhance the formability features. Following the application of the annealing process, the microhardness and crystallography analyses revealed a notable reduction in the amount of microhardness and the intensity of the peaks in the crystal structure, indicating the occurrence of recrystallization. There has been a reduction in the dislocation state and recrystallization. Additionally, this study demonstrated that 600°C is the critical temperature for this composite's recrystallization phenomena. Thus, it can be concluded that the three-layer brass/low carbon steel/brass composite can be made more formable by successfully annealing it at 600°C.

5. References

[1] Vijaya Ramnath, B., Parswajinan, R., Dharmaseelan, K., Thileepan, K. and Nithin Krishna,K. 2021. A review on aluminium metal matrix composites. Materials Today: Proceedings. 46 : 4341-4343. doi:10.1016/j.matpr.2021.03.600.

[2] Sarmah, P. and Gupta, K. 2024. Recent Advancements in Fabrication of Metal Matrix Composites: A Systematic Review. Materials. 17(18):4635. doi:10.3390/ma17184635.

[3] Ikumapayi, O.M., Akinlabi, E.T., Onu, P. and Abolusoro, O.P. 2020. Rolling operation in metal forming: Process and principles . A brief study, Materials Today: Proceedings. 26 :1644-1649. doi:10.1016/j.matpr.2020.02.343.

[4] Soleimanimehr, H. and Nasrollah, A. 2021. A Numerical Investigation the Effects of the Voltage on the Displacement and Stress of Copper-based Ionic Polymer-Metal Composites. Journal of Modern Processes in Manufacturing and Production. 1(10) 77-86. dor:20.1001.1.27170314.2021.10.1.6.5.

[5] Muribwathoho, O., Msomi, V. and Mabuwa, S. 2023.Metal Matrix Composite Developed with Marine Grades: A Review. Materials Science Forum. 1085 :77-89. doi:10.4028/p-jub91t.

[6] Poursafar, A.2019. Analysis of Surface Roughness and Micro-hardness in Roller Burnishing of Aluminum Alloy 6061. Journal of Modern Processes in Manufacturing and Production. 3(8)5-12.

[7] Mortazavi Moghadam, F.s. and Rasouli, S. 2024. Recycling kaolin from paper waste and assessment of its application for paper coating. Materials Today Communications. 39 : 109142. doi:10.1016/j.mtcomm.2024.109142.

[8] Wang, J., Liu, H.-M., Li, S.-F. and Chen, W.-J. 2022. Cold Roll Forming Process Design for Complex Stainless-Steel Section Based on COPRA and Orthogonal Experiment. Materials. 15:8023. doi:10.3390/ma15228023.

[9] Mahdieh, M.S., Nazari, F., Zayed, K.S. and Aghoun, F. 2024. Investigating of Manufacturing of Titanium Hip Prosthesis by Cold Forging Process via FEM Analysis. Journal of Modern Processes in Manufacturing and Production. 3(13) 5-16. Doi:10.71762/z6e6-aw80.

[10] Lin, Y., Cui, X., Chen, K., Xiao, A. and Yan, Z. 2022. Forming Limit and Mechanical Properties of 2024-O Aluminum Alloy Under Electromagnetic Forming. Metals and Materials International. 28(10):2472-2482. Doi:10.1007/s12540-021-01128-x.

[11] Mortazavi Moghadam, F.A., Resalati, H., Rasouli, S. and Asadpour, G. 2021. Fabrication of high mechanical properties papers coated with CMC-based nanocomposites containing nanominerals synthesized from paper waste. Cellulose. 28(17) 11153-11164. doi:10.1007/s10570-021-04241-7.

[12] Kabakçı, M., Karaağaç, İ. and demirel, M. 2019. The experimental investigation of annealing parameters effects on al2024-t3 materials' formability and mechanical properties. European Journal of Technic. 9(2), 338-346. doi:10.36222/ejt.648167.

[13] Mozafari, H. 2024. Numerical and Experimental Analysis of Temperature Field, Deformation, and Residual Stress in Two-Stage Single-Pulse Sub-Powder Welding Joints. Journal of Modern Processes in Manufacturing and Production. 2(13) 47-66. doi:10.71762/dyhz-qx27.

[14] Haji Aboutalebi, F., Farzin, M. and Poursina, M.2011. Numerical simulation and experimental validation of a ductile damage model for DIN 1623 St14 steel. The International Journal of Advanced Manufacturing Technology. 53:157-165. doi:10.1007/s00170-010-2831-z.

[15] Igelegbai, E., Alo, O., Adeodu, A. and Daniyan, I. 2016. Evaluation of Mechanical and Microstructural Properties of α-Brass Alloy Produced from Scrap Copper and Zinc Metal through Sand Casting Process. Journal of Minerals and Materials Characterization and Engineering. 5:18-28. Doi:10.4236/jmmce.2017.51002.

[16] Atay, H., Uslu, G., Kahmaz, Y. and Atay, Ö. 2020. Investigations of microstructure and mechanical properties of brass alloys produced by sand casting method at different casting temperatures. IOP Conference Series: Materials Science and Engineering. 726 :012018. doi:10.1088/1757-899X/726/1/012018.

[17] Tan, P., Sui, Y., Jin, H., Zhu, S., Jiang, Y. and Han, L. 2022. Effect of Zn content on the microstructure and mechanical properties of as-cast Al–Zn–Mg–Cu alloy with medium Zn content. Journal of Materials Research and Technology. 18:2620-2630. doi:10.1016/j.jmrt.2022.03.168.

[18] Utsunomiya ,H. and Matsumoto, R. 2014. Deformation Processes of Porous Metals and Metallic Foams (Review). Procedia Materials Science. 4:234–238. doi:10.1016/j.mspro.2014.07.614.

[19] Motyka, M., Mróz, S., Więckowski, W., Stefanik, A., Ziaja, W., Poręba, M. and Adamus, J. 2024. The influence of the rolling method on cold forming ability of explosive welded Ti/steel sheets. Archives of Civil and Mechanical Engineering. 24(3):191. doi:10.1007/s43452-024-01005-5.

[20] Zarei, E., Afsari, A., Saharkhiz, E. and Osgoui, S.K.G. 2024. Comparison of the Microstructure and Mechanical Behavior of the Welding Zone of Aluminum Alloy 5754 by FSW and TIG Methods. Journal of Modern Processes in Manufacturing and Production. 2(13): 67-84. doi.org/10.71762/7mt5-v498.

[21] Kang, C., Sun, B., Zhang, X. and Yao, C. 2024. Research on the Mechanism and Processability of Roll Forming. Materials. 17 : 3126. doi:10.3390/ma17133126.

[22] Tayyebi, M., Rahmatabadi, D.,. Karimi, .A., Adhami, M. and Hashemi, R. 2021. Investigation of annealing treatment on the interfacial and mechanical properties of Al5052/Cu multilayered

composites subjected to ARB process. Journal of Alloys and Compounds. 871:159513. doi:10.1016/j.matdes.2011.12.045.

[23] Delshad, M., Hashemi, R. and Sedighi, M. 2019. The effect of temperature on the mechanical properties and forming limit diagram of aluminum strips fabricated by accumulative roll bonding process. Journal of Materials Research and Technology. 9(105):4389-4400. doi:10.1007/s00170-019-04586-1.

[24] Mayakannan, S., Muthuraj, M., Ademi, E., Kumar, S.G. , Bhanu Prasad, B. and Ahammad, S.K.H. 2023. Influence of process parameters on microhardness and porosity of Al 2024 microwave cast. Materials Today: Proceedings. 29 (10):212-231. doi:10.1016/j.matpr.2023.05.477.

[25] Raykar, S.J., Chaugule, Y.G., Pasare, V.I., Sawant, D.A. and Patil, U.N. 2022. Analysis of microhardness and degree of work hardening (DWH) while turning Inconel 718 with high pressure coolant environment. Materials Today: Proceedings. 59(1) :1088-1093. doi:10.1016/j.matpr.2022.02.426.

[26] Diehl, M., Kertsch, L., Traka, K., Helm, D. and Raabe, D. 2019. Site-specific quasi in situ investigation of primary static recrystallization in a low carbon steel. Materials Science and Engineering. 755 :295-306. doi:10.1016/j.msea.2019.02.032.

[27] Zhao, Y.H., Bingert, J.F., Topping, T.D., Sun, P.L., Liao, X.Z., Zhu, Y.T. and Lavernia, E.J. 2020. Mechanical Behavior, deformation mechanism and microstructure evolutions of ultrafine-grained Al during recovery via annealing. Materials Science and Engineering. 772:138706. doi:10.1016/j.msea.2019.138706.

[28] Mortazavi Moghadam, F.A., Resalati, H., Rasouli, S. and Asadpour, G. 2022. New method of producing nanominerals from office paper waste and investigating their microstructural properties. Biomass Conversion and Biorefinery. doi:10.1007/s13399-022-02782-w.

[29] Mortazavi Moghadam, F.A., Khoshkalampour, A., Mortazavi Moghadam, F.A., Pourvatan Doust, S., Naeijian, F. and Ghorbani, M. 2023. Preparation and physicochemical evaluation of casein/basil seed gum film integrated with guar gum/gelatin based nanogel containing lemon peel essential oil for active food packaging application. International Journal of Biological Macromolecules. 224:786-796. doi:10.1016/j.ijbiomac.2022.10.166.

[30] Nie, J. , Liu, M., Wang, F., Zhao, Y., Li, Y., Cao, Y. and Zhu, Y. 2016. Fabrication of Al/Mg/Al Composites via Accumulative Roll Bonding and Their Mechanical Properties. Materials. 9(11):951. doi:10.3390/ma9110951.

[31] Ma, X., Li, F., Li, J., Wang, Q., Yuan, Z. and Fang, Y. 2015. Analysis of forming limits based on a new ductile damage criterion in St14 steel sheets. Materials & Design. 68(5):134-145. doi:10.1016/j.matdes.2014.12.029.

[32] Mortazavi Moghadam, F.S. and Mortazavi Moghadam, F.A. 2024. Kombucha fungus bio-coating for improving mechanical and antibacterial properties of cellulose composites. Materials Today Communications. 40:109609. doi:10.1016/j.mtcomm.2024.109609.

[33] Najafizadeh, N., Rajabi, M., Hashemi, R. and Amini, S. 2021. A method and apparatus for determination of the ultrasonic-assisted forming limit diagram, Proceedings of the Institution of Mechanical Engineers, Part C. Journal of Mechanical Engineering Science. 235(23):7062-7073. doi:10.1177/09544062211011509.